EurJIC
European Journal of Inorganic Chemistry

Research Article
doi.org/10.1002/ejic.202200103

Chemistry Europe
European Chemical Societies Publishing

www.eurjic.org

Indenyl and Allyl Palladate Complexes Bearing *N*-Heterocyclic Carbene Ligands: an Easily Accessible Class of New Anticancer Drug Candidates

Thomas Scattolin,*[a] Ilenia Pessotto,[b] Enrico Cavarzerani,[b] Vincenzo Canzonieri,[c, d] Laura Orian,[a] Nicola Demitri,[e] Claudia Schmidt,[f] Angela Casini,[f] Enrica Bortolamiol,[b] Fabiano Visentin,*[b] Flavio Rizzolio,[b, c] and Steven P. Nolan*[g]

The mechanochemical syntheses of allyl and indenyl palladate complexes are reported. All compounds were obtained in quantitative yields and microanalytically pure without the need of any workup. These complexes are stable in chlorinated and polar (DMSO or DMSO/H_2O solutions) solvents. In chlorinated solvents, they appear as ionic pairs of which crystals suitable for single X-ray diffraction studies have been obtained. Bonding and solvation properties are rationalized through scalar relativistic DFT calculations. Moreover, most complexes showed excellent cytotoxicity towards ovarian cancer cell lines, with IC_{50} values comparable or lower than cisplatin. The potent anticancer activity of two IPr^{Cl} and IPr*-based palladate complexes was examined in a high-grade serous ovarian cancer (HGSOC) patient-derived tumoroid. Moreover, the inhibition of the antioxidant enzyme thioredoxin reductase (TrxR) was noticed, and structure-activity relationships could be derived, suggesting the ROS detoxifying system is involved in the mode of action.

Introduction

As a result of the introduction of cisplatin as a commercially available potent anticancer drug, the role of inorganic chemists has been crucial in the development of modern medicinal chemistry.[1] In this context, the approval of second and third generations platinated chemotherapeutic agents (carboplatin and oxaliplatin) showing reduced side-effects than the parent cisplatin, was a significant advance in the field. However, even these compounds have a non-negligible collateral toxicity[2] and above all, they are inactive against some classes of tumors resistant to cisplatin.[3] These clinical findings have led researchers to develop alternative or complementary therapeutic approaches such as radiotherapy, immunotherapy and photodynamic/photothermal therapies, as well as the synthesis and study of the anticancer properties of compounds containing metals other than platinum.[4] The most encouraging results have been obtained with gold[5] and ruthenium[6] complexes, although few examples of these have so far completed clinical approval as anticancer drugs.

Organopalladium compounds have recently attracted attention for their high stability even under physiological conditions and above all for their remarkable *in vitro* cytotoxicity towards cisplatin-resistant cell lines.[7] Among the organopalladium derivatives, those bearing at least one *N*-heterocyclic carbene ligand (NHC) and the Pd(II)-η^3-allyl fragment have exhibited IC_{50} values in the micro- and sub-micromolar range towards several cisplatin-sensitive and cisplatin-resistant cell lines *in vitro* and in

[a] *Dr. T. Scattolin, Prof. Dr. L. Orian*
Dipartimento di Scienze Chimiche,
Università degli studi di Padova
Via Marzolo 1, 35131 Padova, Italy
E-mail: thomas.scattolin@unipd.it
https://www.organometallics.it
[b] *I. Pessotto, E. Cavarzerani, E. Bortolamiol, Prof. Dr. F. Visentin, Prof. Dr. F. Rizzolio*
Dipartimento di Scienze Molecolari e Nanosistemi,
Università Ca' Foscari
Campus Scientifico Via Torino 155, 30174 Venezia-Mestre, Italy
E-mail: fvise@unive.it
https://www.unive.it/data/people/5590498/didattica_prec
[c] *Prof. Dr. V. Canzonieri, Prof. Dr. F. Rizzolio*
Pathology Unit, Department of Molecular Biology and Translational Research,
Centro di Riferimento Oncologico di Aviano (CRO) IRCCS
Via Franco Gallini 2, 33081 Aviano, Italy
[d] *Prof. Dr. V. Canzonieri*
Department of Medical, Surgical and Health Sciences,
Università degli Studi di Trieste
Strada di Fiume 447, 34137 Trieste, Italy
[e] *Dr. N. Demitri*
Area Science Park
Elettra-Sincrotrone Trieste, S. S. 14 Km 163.5, Basovizza, 34149 Trieste, Italy
[f] *Dr. C. Schmidt, Prof. Dr. A. Casini*
Chair of Medicinal and Bioinorganic Chemistry,
Department of Chemistry, Technical University of Munich
Lichtenbergstr. 4, 85748 Garching b. München, Germany
[g] *Prof. Dr. S. P. Nolan*
Department of Chemistry and Centre for Sustainable Chemistry,
Ghent University
Krijgslaan 281, S–3, 9000 Ghent, Belgium
E-mail: steven.nolan@ugent.be
https://www.nolan.ugent.be

Supporting information for this article is available on the WWW under https://doi.org/10.1002/ejic.202200103

Part of the "EurJIC Talents" Special Collection.

Research Article
doi.org/10.1002/ejic.202200103

some cases selectivity towards cancerous vs non-tumorigenic cells.[8]

An unusual family of Pd(II)-allyl derivatives, whose antiproliferative properties has not been examined thus far, is that of the palladate type [NHC·H][$PdCl_2$(R-allyl)] (R-allyl = allyl, 2-Me-allyl and cinnamyl). These compounds have been isolated for the first time in 2017 and represent the key intermediate in obtaining well-defined [Pd(NHC)Cl(R-allyl)] precatalysts when a generic imidazolium salt is reacted with the precursor [Pd(μ-Cl)(R-allyl)]$_2$ in the presence of a weak base (*e.g.* K_2CO_3) (Scheme 1).[9] This approach, known as the *weak-base route*, represents the simplest and most environmentally sustainable route to achieve metal-NHC complexes.[10]

The surprising stability to air and moisture of the palladate intermediates has allowed their study as potential precatalysts in C–C and C–N coupling reactions, showing excellent performance and a broad functional group tolerance in the presence of mild inorganic bases and green solvents.[11] Another important advantage of these derivatives is that they can be easily prepared on a gram scale under solvent-free conditions and without the need of any workup.[11] For all these reasons, we believe that a computational study on the nature of the palladate-NHC interaction and the evaluation of the anticancer activity of these complexes could be of great interest.

Furthermore, with the aim of understanding the role of organopalladium fragment in the antitumor activity of these systems, the syntheses and biological activity of indenyl palladate complexes has also been explored (vide infra). It should be remembered that the reactivity of the indenyl fragment is sometimes quite different from that of the allyl congener (*indenyl effect*) as previously demonstrated in numerous reports.[12] In addition, the biological properties of metal-indenyl complexes have been scarcely explored compared to those of their allyl relatives.[13]

Thomas Scattolin was born in Padua (Italy) in 1990 and studied chemistry at the Ca' Foscari University of Venice (BSc 2012 and MSc 2014, summa cum laude). He completed his PhD in 2019 under the supervision of Prof. Fabiano Visentin in the same university (inter-university programme with University of Trieste). In 2018 he was a visiting scientist in the laboratories of Prof. Antonio Togni at the ETH in Zurich, Switzerland. In 2020, he joined the laboratory of Prof. Steven P. Nolan at the Ghent University. In 2021, he worked as postdoc researcher at CRO Aviano, Italy, within the CaTHENa project (Cancer THErapy by Nanomedicine). Since 2022 he is assistant professor in Inorganic Chemistry at the University of Padova. His research activity is primarily focused on the synthesis and reactivity of late transition metal complexes with applications in homogeneous catalysis and medicinal chemistry.

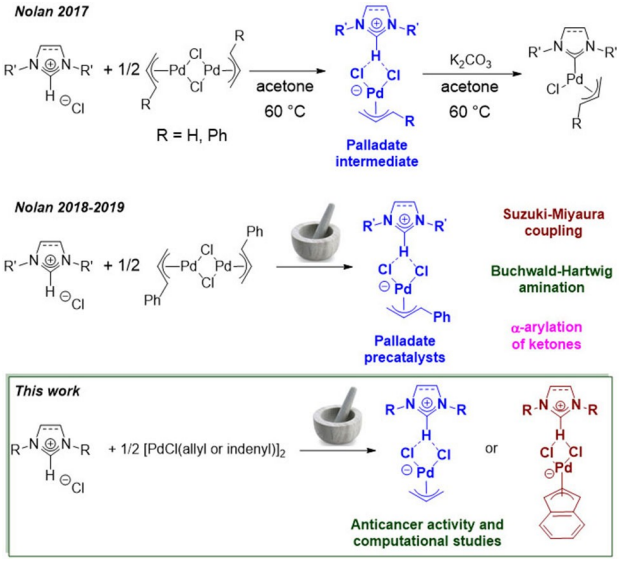

Scheme 1. Palladate complexes bearing NHC ligands as reaction intermediates, efficient precatalysts and potent anticancer agents.[9,11]

Results and Discussion

Mechanochemical Synthesis of Allyl and Indenyl Palladates

Based on the procedure recently reported by Nolan and co-workers for the preparation of cinnamyl palladates, a selection of [NHC·H][Pd(allyl)Cl_2] complexes were synthesized using the solvent-free method consisting of simply grinding the [Pd(allyl)(μ-Cl)]$_2$ precursor with different saturated and unsaturated azolium salts (NHC·HCl, **1a–f**). Complexes **2a–f** were obtained quantitatively and fully characterized by means of NMR, XRD and elemental analyses (Scheme 2). Except for **2a**, which was synthesized in 2017 using acetone as a solvent,[9] all other compounds are novel and unreported to date.

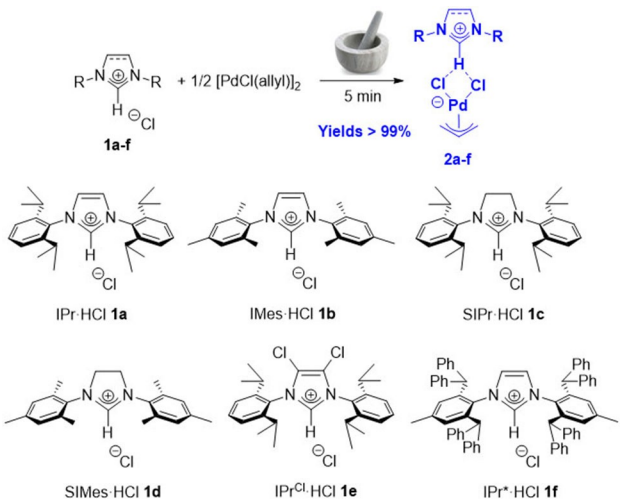

Scheme 2. Solvent-free synthesis of allyl palladate complexes **2a–f**.

Research Article
doi.org/10.1002/ejic.202200103

In the ^{1}H NMR spectra, the imidazole proton NCHN is shifted by ca. 2 ppm with respect to the starting azolium salt. Regarding the allyl fragment, three sets of signals can be found and are attributed to the *anti* (doublet at 2.56–2.86 ppm with $J \approx 12$ Hz), *syn* (doublet at 3.75–3.88 ppm with $J = 6$–7 Hz) and *central* allyl protons (multiplet at 5.10–5.30 ppm). Similarly, in the ^{13}C NMR spectra, the signals of the allyl carbons (CH_2 and CH at ca. 61 and 110 ppm, respectively), the imidazole carbon NCHN (ca. 140 ppm for **2a**–**b** and **2e**–**f**, and ca. 160 ppm for **2c**–**d**) and the remaining signals of the imidazole fragment can be clearly identified. To further confirm the nature of the synthesized allyl complexes, the X-ray structure of **2f** was obtained by single crystal X-ray diffraction (Figure 1). Suitable crystals were grown by slow vapour diffusion of diethylether into $CHCl_3$ solution.

The reaction between the imidazolium salts **1a**–**f** and the precursor [Pd(indenyl)(μ-Cl)]$_2$ was carried out using the same mechanochemical procedure. In all cases, the final compounds **3a**–**f** were obtained in quantitative yields and high purity (Scheme 3).

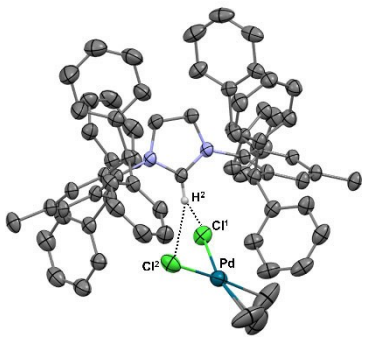

Figure 1. X-ray molecular structure of **2f** is presented, showing thermal displacement ellipsoids at the 50% probability level with $CHCl_3$ (solvent molecule) and hydrogen atoms omitted for clarity. CCDC: 2150854.

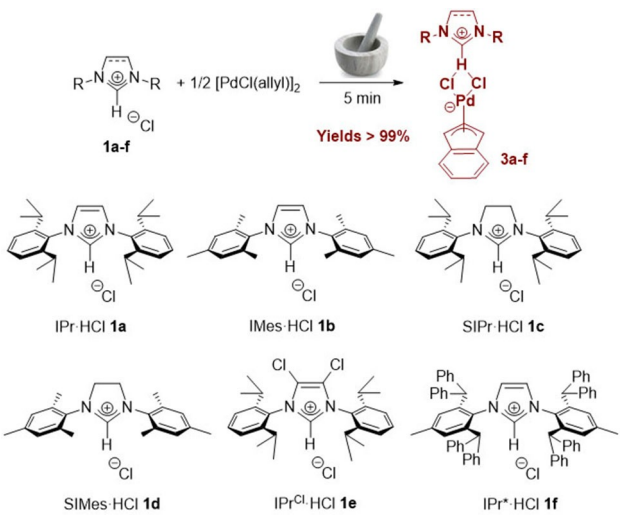

Scheme 3. Solvent-free synthesis of indenyl palladate complexes **3a**–**f**.

Similarly to the allyl derivatives **2a**–**f**, the ^{1}H NMR spectra of the indenyl complexes **3a**–**f** show the NCHN imidazole proton at chemical shift significantly lower than that of the starting material. Moreover, the four different indenyl signals are easily identified: $H^{1,3}$ (doublet at 5.44–5.70 ppm with $J \approx 3$ Hz), H^2 (triplet at 6.45–7.00 ppm with $J \approx 3$ Hz), $H^{4,7}$ and $H^{5,6}$ (multiplets at 6.50–7.00 ppm). In the ^{13}C NMR spectra, the most diagnostic signals are that ascribable to the imidazole carbon NCHN (ca. 140 ppm for **3a**–**b** and **3e**–**f**, and ca. 160 ppm for **3c**–**d**) and those of indenyl carbons: $C^{1,3}$ (76–77 ppm), C^2 (ca. 110 ppm), $C^{5,6}$ (ca. 118 ppm), $C^{4,7}$ (ca. 126 ppm) and $C^{3a,7a}$ (ca. 141 ppm). Notably, the position of the $C^{3a,7a}$ signals, following the model proposed by Baker and Tulip,[14] is an index of the hapticity assumed by the indenyl fragment. Specifically, the hapticity can be correlated with the difference in chemical shift (in ppm) between the $C^{3a,7a}$ signal of the complex of interest and the same signal in the reference compound NaInd (130.7 ppm). If the value of $\Delta\delta$ assumes clearly positive values, then the indenyl fragment assumes a η^3 hapticity. Conversely, if this value presents clearly negative values ($\Delta\delta < 0$), the indenyl fragment assumes a η^5 hapticity. Complexes **3a**–**f** present $\Delta\delta$ values around 10 ppm, therefore their hapticity can be considered intermediate between η^3 and η^5, with a greater η^3 character. Finally, the structure of complex **3b** was unequivocally confirmed by single crystal X-ray diffraction (Figure 2).

Both allyl and indenyl palladates are stable in $CDCl_3$ as well as in a 1:1 DMSO-d^6/D_2O solution (see ESI). The latter data are of importance as biological tests are carried out by adding appropriate amounts of a DMSO solution of the complex to the cellular medium. Intriguingly, the ^{1}H NMR spectra of indenyl palladates **3a**–**f** recorded in DMSO-d^6/D_2O showed perfectly superimposable indenyl signals between the various complexes examined (see ESI). This means that the indenyl complexes **3a**–**f** exist as pairs of solvated ions in this mixture of polar solvents. Conversely, the allyl complexes **2a**–**f** maintain their original structure or undergo only partial dissociation in DMSO-d^6/D_2O solution (see ESI).

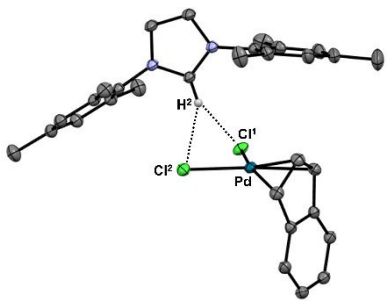

Figure 2. X-ray molecular structure of **3b** is presented, showing thermal displacement ellipsoids at the 50% probability level with most of the hydrogen atoms and $CHCl_3$ (solvent molecule) omitted for clarity. CCDC: 2150853.

Research Article
doi.org/10.1002/ejic.202200103

Computational Studies

Intrigued by the surprising stability of allyl and indenyl palladates, and their different behaviour in solvents with varied polarity, we undertook a computational analysis on the nature of the H···Cl bifurcated interaction between the azolium moiety and the allyl/indenyl palladate. Preliminarily, the geometries of complexes **2a** and **3a** have been fully optimized at ZORA-BLYP-D3(BJ)/TZ2P level of theory (see Computational details), starting from the crystal structure of [IPr·H][$PdCl_2$(cinnamyl)][9] and replacing the cinnamyl ligand with the allyl and indenyl moieties, respectively. The results are shown in Figure 3.

Activation strain analysis has been used to investigate the energetics and the nature of the H···Cl bonds, by partitioning each complex into two charged fragments; the natural choice for the fragments was the allyl/indenyl palladate (Fragment 1) and the azolium moiety (Fragment 2). The results are shown in Table 1. In both cases, the ΔE_{strain} is small and comparable. The total interaction is larger in **2a** than in **3a** despite the two H–Cl distances are similar in the two complexes. Energy decomposition analysis (Table 1) reveals that this must be ascribed to a decrease of the stabilizing ΔV_{elstat} and ΔE_{disp} (in absolute value) when going from **2a** to **3a**, which is not balanced by the decrease in ΔE_{Pauli}. When comparing **2a** to **3a**, one can infer the clear difference between allyl and indenyl ligands is due to the ΔV_{elstat} which results in stabilizing by ca. 5 kcal mol^{-1} the former complex.

In **2a** and **3a**, the H···Cl interactions are non-equivalent, as can be appreciated on a basis of the observed geometric, because one H–Cl distance is systematically shorter by ~0.4–0.5 Å.

Q_A^{VDD} is more negative for the chlorine at the shorter distance and both Cl atoms have a more negative charge in the allyl **2a** than in the indenyl complex **3a** (Table 2). The charge transfer from the azolium H to the halogens is inferred computing the values of ΔQ_H^{VDD} (see Experimental Section), i.e., 0.032 in **2a** and 0.029 in **3a**, respectively.

To gain insight into the behaviour of **2a** and **3a** in solution, we have fully computationally optimized geometries of both complexes in $CHCl_3$, in DMSO and in water, using a continuum approach to describe the polar environment (level of theory: COSMO-ZORA-BLYP-D3(BJ)/TZ2P). In all cases, the energy of the entire complex is compared to the sum of the energies of its ion fragments, these latter being always more stable, as expected in solution (Table 3). The stabilization of **2a** and **3a** decreases with increasing medium polarity, that is, when going from $CHCl_3$ to DMSO and to water, the fragmentation is energetically favoured. The energy trend is accompanied by a progressive elongation of the H···Cl interatomic distances indicating that this interaction becomes weaker (Figure S1). The complex fragmentation is slightly more favoured for **3a** than for **2a**, in qualitative agreement with the experimental findings. The effect of including explicit solvent molecules has been investigated in chloroform and water using the semiempirical quantum mechanical method GFN2-xTB[15] and details are provided in the Supporting Information. The same trend is observed and the effect of weakening of the H···Cl interaction is more evident in **3a** than in **2a**.

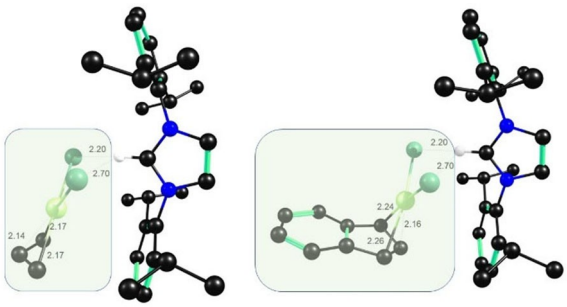

Figure 3. Fully optimized structures of **2a** (left) and **3a** (right). Level of theory: ZORA-BLYP-D3(BJ)/TZ2P. All hydrogen atoms, except H involved in the H···Cl bifurcated interaction, have been omitted in the representation for sake of clarity. Interatomic distances are in Å.

Table 1. ASA and EDA for the studied complexes; all values are in kcal mol^{-1}. Level of theory: ZORA-BLYP-D3(BJ)/TZ2P.

	ΔE_{strain}	ΔE_{int}	ΔE_{oi}	ΔV_{elstat}	ΔE_{Pauli}	ΔE_{disp}	ΔE
2a	2.57	−95.67	−29.80	−91.74	51.45	−25.58	−93.10
3a	2.76	−92.21	−29.50	−86.86	48.76	−24.61	−89.45

X-Ray Diffraction Analysis

3b crystalline form bears one crystallographically independent palladium complex in the crystallographic asymmetric unit, while **2f** shows two distinct entities (Figure S3–4). Solvent molecules (chloroform and diethyl ether) have been found in both the crystal packing voids. Palladium centres show square planar coordination spheres (Tables S9), in agreement with previously published data. Entries deposited on CSD database (5.43 - November 2021 version), containing the [(η^3-R-allyl)$PdCl_2$]$^-$ fragment, show equivalent average geometrical parameters ($d_{Pd\cdots Cl}$ = 2.39(1) Å, $\Lambda_{Cl\cdots Pd\cdots Cl}$ = 95.6(2.0)°, $d_{Pd\cdots C=C}$ = 2.12(3) Å, $\Lambda_{C=C\cdots Pd\cdots C=C}$ = 68.9(0.8)°).

Table 2. Voronoi deformation densities (Q_A^{VDD}) for the atoms involved in the intramolecular hydrogen bond. Level of theory: ZORA-BLYP-D3(BJ)/TZ2P.

Complex	Cl	Cl	H
2a	−0.406	−0.403	0.061
3a	−0.392	−0.388	0.061

Table 3. Energies (kcal mol^{-1}) of **2a** and **3a** in $CHCl_3$, DMSO and H_2O; all values are relative to the sum of the energies of the corresponding ion fragments. Level of theory: COSMO-ZORA-BLYP-D3(BJ)/TZ2P.

Complex	$CHCl_3$	DMSO	H_2O
2a	−30.4	−15.4	−14.4
3a	−29.7	−15.0	−14.0

Two similar "ate" complexes have been previously published and the overall molecular arrangement is well conserved as shown with overlapped models in Figure S5.[9] Average R.M.S.D. is less than ~1 Å, among palladate common atoms and only minor rearrangements are found in the **2f** fragments and the closely related CCDC 1439390 molecule (i.e. bearing the same imidazolium cation).

A strong ion-pair is formed in the solid-state, between the most acidic proton of the imidazolium heterocycle and chloride ligands of the palladate. The bulkiness of imidazolium moieties and crystal packing effects disturb the angle between the ions but the reciprocal orientation and distance between relevant atoms is almost constant (average $d_{C\text{-}H\cdots ClPd} = 3.37(6)$ Å). Similar strong polar contacts keep solvent chloroform molecules tightly bound to the palladate moieties ($d_{CH\cdots Cl} = 3.765(3)$ Å in **3b** and $d_{CH\cdots Cl} = 3.403(1)$ Å in **2f**). Crystal packing shows also hydrophobic contacts among neighbour molecules, involving weak intermolecular π···π and several CH···π interactions, among neighbour ligand phenyl sidechains.

Antiproliferative Activity on Ovarian Cancer Cell Lines

The high stability in solution of allyl and indenyl palladates combined with the straightforward and sustainable protocol for their synthesis represent ideal requirements for a potential metallodrug. Based on the encouraging biological results obtained with some well-defined palladium allyl complexes, we wondered if even these simple palladates are able to inhibit the proliferation of tumor cells. To this end, a selection of three different human ovarian cancer cell lines (OVCAR5, A2780, and its cisplatin resistant clone A2780*cis*) were treated with our compounds and cisplatin (positive control).

The antiproliferative activity data obtained in the above-mentioned cell lines are reported in Table 4 in terms of IC_{50} values (half inhibitory concentrations).

Based on the IC_{50} values obtained, we can draw some interesting conclusions. First, it is possible to observe that most of the tested compounds show cytotoxicity in the micro- and sub-micromolar range, with a comparable activity between allyl derivatives and their indenyl congeners. Regarding the effect of the imidazole moiety, the complexes bearing saturated azolium salts (**2c–d** and **3c–d**) are generally less active than their unsaturated congeners (**2a–b** and **3a–b**). An exception to this trend is represented by complex **2d**, which exhibits a remarkable cytotoxicity towards A2780 and A2780*cis* cells.

On the contrary, the introduction of electron-withdrawing groups in the backbone or an increase of steric hindrance seems to significantly raise the antiproliferative activity in the tumor cell lines. Indeed, complexes **2e–f** and **3e–f**, bearing IPr^{Cl} and IPr*-based azolium salts, respectively, are much more active than the unsubstituted IPr analogues **2a** and **3a**.

Analyzing each cell line, it is possible to observe that in A2780 cells most of the complexes exhibit cytotoxicity comparable or even superior to cisplatin. A similar result was obtained on OVCAR5 cells (high-grade serous ovarian cancer), in which the high antiproliferative activity of IPr^{Cl} and IPr* derivatives (**2e–f** and **3e–f**) and the substantial inactivity of SIMes and SIPr complexes **2c** and **3d** are noteworthy. Particularly interesting are the results obtained in the cisplatin-resistant cell line (A2780*cis*), as most of the palladates exhibited IC_{50} values up to two orders of magnitude lower than cisplatin. Curiously, in most cases the IC_{50} values between the A2780 and A2780*cis* lines are comparable, suggesting a different mechanism of action than that of cisplatin.

In summary, seven compounds (**2a**, **2b**, **2c**, **2e**, **2f**, **3e** and **3f**) showed higher cytotoxicity than the benchmark cisplatin in all ovarian cancer cell lines examined. Four of these, as previously mentioned, are IPr^{Cl} and IPr*-based allyl and indenyl palladates.

Table 4. IC_{50} (μM) of allyl and indenyl palladates and cisplatin on cancer cell lines recorded after 96 h incubation.[a]

Complex	A2780	A2780cis	OVCAR5
Cisplatin	**0.3 ± 0.1**	**20 ± 3**	**3.4 ± 0.9**
[IPr·H][$PdCl_2$(allyl)] (**2a**)	0.33 ± 0.08	2.04 ± 0.06	0.6 ± 0.4
[IMes·H][$PdCl_2$(allyl)] (**2b**)	0.08 ± 0.03	0.7 ± 0.2	1.7 ± 0.2
[SIPr·H][$PdCl_2$(allyl)] (**2c**)	3.9 ± 0.3	16 ± 6	> 100
[SIMes·H][$PdCl_2$(allyl)] (**2d**)	0.04 ± 0.01	0.79 ± 0.06	5.30 ± 0.09
[IPr^{Cl}·H][$PdCl_2$(allyl)] (**2e**)	0.12 ± 0.04	0.17 ± 0.06	0.5 ± 0.1
[IPr*·H][$PdCl_2$(allyl)] (**2f**)	0.19 ± 0.07	0.2 ± 0.1	0.08 ± 0.02
[IPr·H][$PdCl_2$(indenyl)] (**3a**)	0.55 ± 0.02	0.78 ± 0.02	6 ± 1
[IMes·H][$PdCl_2$(indenyl)] (**3b**)	0.3 ± 0.1	3 ± 2	9 ± 1
[SIPr·H][$PdCl_2$(indenyl)] (**3c**)	1.4 ± 0.1	2.9 ± 0.1	4.2 ± 0.7
[SIMes·H][$PdCl_2$(indenyl)] (**3d**)	1.5 ± 0.2	21 ± 5	> 100
[IPr^{Cl}·H][$PdCl_2$(indenyl)] (**3e**)	0.17 ± 0.06	0.24 ± 0.04	0.8 ± 0.2
[IPr*·H][$PdCl_2$(indenyl)] (**3f**)	0.08 ± 0.01	0.09 ± 0.01	0.02 ± 0.01

[a] Stock solutions in DMSO for all complexes; stock solutions in H_2O for cisplatin. A2780 (cisplatin-sensitive ovarian cancer cells), A2780*cis* (cisplatin-resistance ovarian cancer cells) and OVCAR-5 (high-grade serous ovarian cancer cells).

Antiproliferative Activity on a High-Grade Serous Ovarian Cancer Tumoroid

The promising antiproliferative activity exerted by allyl and indenyl palladates towards classical ovarian cancer cell lines has prompted us to investigate some of the most active compounds on a more complex biological model. Taking advantage of organoid technology, one high-grade serous ovarian cancer (HGSOC) tumoroid derived from ascites sites (**Patient A**), recently extracted from a patient and characterized by some of us,[16] was selected to test the efficacy of IPr*-based allyl and indenyl palladates **2f** and **3f**. It is helpful to recall that about 30% of HGSOC patients develop ascites, which are free-floating cells that are responsible for intraperitoneal metastasis.[17] Such patients are difficult to treat with classic chemotherapy and paracentesis is used to alleviate their symptoms.[18]

With the aim of testing the drugs currently available on the market as well as new promising anticancer agents, the use of organoids, which are lab-built mini-organs that can act as models to reconstitute cancer development, is now a widespread technology.[19] A few leading groups in this field are developing animal and *ex vivo* organoid models of ovarian cancer to better replicate the response of clinical patients.[20]

Research Article
doi.org/10.1002/ejic.202200103

Such efforts have allowed the creation of biobanks of organoids, that represent the latest frontier in *ex vivo* testing of drugs.[21]

Considering this information, herein we report the antiproliferative activity exhibited by the palladates species **2f** and **3f** against the tumoroid present in our biobank, expressing their cytotoxicity in terms of IC_{50} values (Table 5).

The IC_{50} values obtained on this HGSOC patient-derived tumoroid confirm the excellent anticancer activity of this category of easily accessible complexes, with half inhibitory concentrations in the sub-micromolar range. At the same time, the result obtained with carboplatin, which is the reference compound for clinical standard therapy, testifies to the high resistance of ascites to classical platinum-based anticancer drugs.

These results suggest the possible application of allyl/indenyl palladates in chemotherapy and heavily treated patients who are resistant to most of the commercially available drugs.

Inhibition of Thioredoxin Reductase (TrxR) Enzymes

As anticipated in the introductory section, in some recent contributions we have demonstrated the promising anticancer activity of cationic palladium complexes of the type [Pd(NHC)(PTA)(allyl)]X (PTA = 1,3,5-triaza-7-phosphaadamantane and X = BF_4, ClO_4).[8] Conversely, their neutral precursors [Pd(NHC)Cl(allyl)] exhibited less promising cytotoxicity. Preliminary investigations on the mechanism of action of palladium allyl complexes, conducted using immunofluorescence techniques, have shown an early mitochondrial dysfunction of the treated tumor cells and the subsequent activation of the apoptosis process, with consequent damage to other cellular organelles.[8a]

Intrigued by the marked antitumor activity of the anionic allyl palladates [NHC·H][$PdCl_2$(allyl)] reported in this work, we wondered if a comparison between these three different categories of palladium complexes can go beyond the simple antiproliferative activity. With this aim, we tested two compounds from each family, bearing the popular IPr and IMes ligands, as potential inhibitors of thioredoxin reductase (TrxR) enzymes (see Scheme 4).

This class of proteins is contained both in bacteria and animals (including humans) and, albeit with some structural differences, this is the only class of proteins capable of reducing thioredoxin in living systems.[22] This chemical event plays a key role in cellular metabolism as demonstrated by the overexpression of these proteins in tumor cells, to cope with an altered and inefficient metabolism that leads to a greater demand for glucose for proliferation (Warburg effect). Moreover, TrxR enzymes were found to be one of the main molecular targets of promising gold-based antitumor and antibacterial agents.[23] Conversely, little attention has been paid to biologically active palladium complexes as potential TrxR inhibitors.

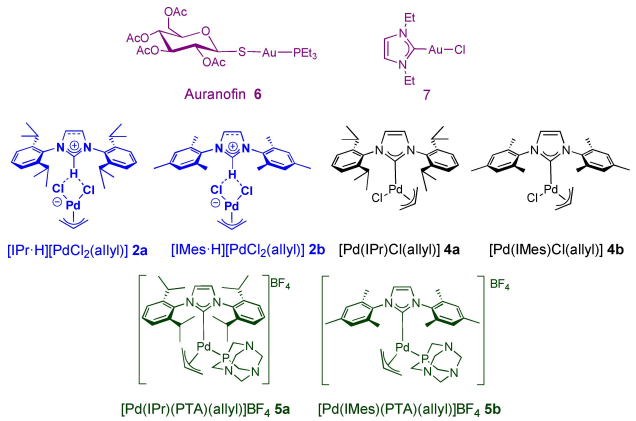

Scheme 4. Compounds tested as inhibitors of bacterial TrxR.

In this context, we evaluated the inhibitory activity exerted by the six selected palladium complexes on the commercially available model protein TrxR (from *E. Coli*). Auranofin (**6**) and the gold(I) NHC complex **7** were chosen as references due to their strong and well-known ability of inhibiting this bacterial protein (Scheme 4).[24]

From the results summarized in Table 6 it is possible to observe the remarkable inhibitory activity of allyl palladates **2a**–**b**, which is significantly higher than that of both Auranofin and gold(I) NHC complex **7**. Interesting EC_{50} values in the sub-micromolar range were also obtained for the neutral and cationic complexes **4a**–**b** and **5a**–**b**. In all cases, the activity of IPr-based complexes is superior to that of their IMes congeners. Curiously, the trend [NHC·H][$PdCl_2$(allyl)] > [Pd(NHC)(PTA)(allyl)]BF_4 > [Pd(NHC)Cl(allyl)] is in agreement with that observed for their *in vitro* anticancer activity.

Table 5. IC_{50} (μM) of allyl/indenyl palladates and carboplatin on ovarian cancer tumoroid after 96 h of incubation.

Complex	Patient A
Carboplatin	> 200
[IPr*·H][$PdCl_2$(allyl)] (**2f**)	0.4 ± 0.2
[IPr*·H][$PdCl_2$(indenyl)] (**3f**)	0.3 ± 0.1

Table 6. Inhibition of bacterial thioredoxin reductase (TrxR) as EC_{50} values. Incubation for 75 min at 25 °C, measured in triplicate.

Complex	EC50 [μM])[a]
Auranofin (**6**)[24a]	0.296 ± 0.069*
Au(I)–NHC complex **7**[24a]	0.108 ± 0.0280
[IPr·H][$PdCl_2$(allyl)] (**2a**)	0.018 ± 0.003
[IMes·H][$PdCl_2$(allyl)] (**2b**)	0.027 ± 0.004
[Pd(IPr)Cl(allyl)] (**4a**)	0.482 ± 0.123
[Pd(IMes)Cl(allyl)] (**4b**)	0.579 ± 0.023
[Pd(IPr)(PTA)(allyl)]BF_4 (**5a**)	0.115 ± 0.020
[Pd(IMes)(PTA)(allyl)]BF_4 (**5b**)	0.322 ± 0.068

[a] Incubation for 75 min at 25 °C, measured in triplicate.

Research Article
doi.org/10.1002/ejic.202200103

Conclusion

In summary, we have prepared a wide-range of allyl and indenyl palladate complexes using a solvent-free method consisting of grinding the corresponding palladium precursors with different saturated and unsaturated azolium salts. The final compounds were obtained without further purification in quantitative yields and were exhaustively characterized by NMR, elemental analysis and XRD. Both allyl and indenyl palladates are stable in $CDCl_3$ as well as in a 1:1 DMSO-d^6/D_2O solution. Curiously, the indenyl complexes **3a**–**f** exist as pairs of solvated ions in DMSO-d^6/D_2O. Conversely, their allyl congeners **2a**–**f** maintain their original structure or undergo only partial dissociation under the same conditions. **2a** and **3a** were selected as model systems to investigate their relative stability, which is higher in the former mainly due to electrostatic interaction, although in both species the azolium and palladate fragments are significantly stabilized by dispersion. The intramolecular H···Cl interaction has been elucidated and quantified using the Voronoi Deformation Density scheme. Importantly, the decreasing stability of both complexes has been observed in solvents of different polarity, as evidenced on energy basis and by elongation of H···Cl interatomic distances. This result is more pronounced for **3a**, in qualitative agreement with the experiment.

Finally, most of the complexes showed excellent cytotoxicity towards ovarian cancer cell lines, with IC_{50} values comparable or lower than cisplatin. Among the various compounds tested, those that exhibited the best antitumor activity contain the IPr^{Cl} or IPr*-based imidazolium moiety. Interestingly, the potent anticancer activity was also confirmed in a high-grade serous ovarian cancer (HGSOC) patient-derived tumoroid, with a clear superiority of this class of compounds over classical platinum-based agents (cisplatin and carboplatin).

Preliminary enzyme inhibition studies of the Pd(II) complexes against the model TrxR show that the compounds have high activity comparable to or even higher than auranofin and classical Au(I) NHC complexes. The obtained results also suggest that enzyme inhibition occurs following protein binding via ligand exchange reaction at the Pd(II) centre, as it is typical of many enzyme-inhibiting metallodrugs, including Au(I) NHC complexes.[25]

Based on such promising data, further *in vitro* and *in vivo* experiments and in-depth mechanistic studies are ongoing in our laboratories.

Experimental Section

General Information

The palladium precursors $[Pd(allyl)(\mu\text{-}Cl)]_2$ and $[Pd(indenyl)(\mu\text{-}Cl)]_2$,[26] gold(I) complex **7**,[24b–c] and [Pd(IPr/IMes)Cl(allyl)] complexes **4a**–**b**[9,27] were synthesized according to previously published procedures. Other reagents were purchased and used as received without further purification, unless otherwise stated.

^1H, $^{13}C\{^1H\}$ NMR and bidimensional (HSQC, HMBC) spectra were recorded on a Bruker Advance 400 spectrometer at room temperature (298 K). The IR spectra were recorded on a Perkin-Elmer Spectrum One spectrophotometer and elemental analysis was carried out using an Elemental CHN "CUBO Micro Vario" analyzer. X-ray intensity data were collected at 100 K at the XRD2 beamline of the Elettra Synchrotron, Trieste (Italy). The human cancer cell lines tested were purchased from Sigma-Aldrich.

General Procedure

In air, the azolium salt (NHC·HCl) and the dimeric precursors $[Pd(allyl)(\mu\text{-}Cl)]_2$ or $[Pd(indenyl)(\mu\text{-}Cl)]_2$ were added to a mortar. The two solids were mixed and grinded using a pestle for 5 min. A yellow/brownish powder was obtained.

Synthesis of [IPr·H][PdCl$_2$(allyl)] (2a)

Following the general procedure from IPr·HCl (65.0 mg, 0.153 mmol) and $[Pd(allyl)(\mu\text{-}Cl)]_2$ (28.0 mg, 0.0765 mmol), the product was obtained as a pale-yellow powder in a quantitative yield.

^1H-NMR (400 MHz, $CDCl_3$, T = 298 K, ppm) δ: 1.22 (d, J = 6.9 Hz, 12H, $CH_{3(IPr)}$), 1.29 (d, J = 6.9 Hz, 12H, $CH_{3(IPr)}$), 2.50 (hept, J = 6.9 Hz, 4H, $C\underline{H}(CH_3)_2$), 2.76 (d, J = 12.0 Hz, 2H, *anti* allyl-H), 3.85 (d, J = 6.7 Hz, 2H, *syn* allyl-H), 5.23 (m, 1H, *central* allyl-H), 7.34 (d, J = 7.8 Hz, 4H, *m*-$H_{(IPr)}$), 7.56 (t, J = 7.8 Hz, 2H, *p*-$H_{(IPr)}$), 8.34 (d, J = 1.6 Hz, 2H, $CH{=}CH_{Im}$), 9.08 (t, J = 1.6 Hz, 1H, NCHN).

$^{13}C\{^1H\}$-NMR ($CDCl_3$, T = 298 K, ppm) δ: 24.1 (CH_3, $CH_{3(IPr)}$), 24.8 (CH_3, $CH_{3(IPr)}$), 29.2 (CH, $\underline{CH}(CH_3)_2$), 61.0 (CH_2, allyl-CH_2), 109.5 (CH, allyl-CH), 124.8 (CH, *m*-$CH_{(IPr)}$), 127.8 (CH, $CH{=}CH_{Im}$), 130.1 (C, *o*-$C_{(IPr)}$), 132.2 (C, *p*-$C_{(IPr)}$), 137.0 (CH, NCHN), 145.3 (CH, *i*-$CH_{(IPr)}$).

Analytical Data Obtained are in Agreement with Reported Values[9]

Synthesis of [IMes·H][PdCl$_2$(allyl)] (2b)

Following the general procedure from IMes·HCl (65.0 mg, 0.191 mmol) and $[Pd(allyl)(\mu\text{-}Cl)]_2$ (34.9 mg, 0.0954 mmol), the product was obtained as a pale-yellow powder in a quantitative yield.

^1H-NMR (400 MHz, $CDCl_3$, T = 298 K, ppm) δ: 2.22 (s, 12H, *o*-$CH_{3(IMes)}$), 2.34 (s, 6H, *p*-$CH_{3(IMes)}$), 2.59 (d, J = 12.0 Hz, 2H, *anti* allyl-H), 3.77 (d, J = 6.7 Hz, 2H, *syn* allyl-H), 5.13 (m, 1H, *central* allyl-H), 7.02 (s, 4H, *m*-$H_{(IMes)}$), 7.52 (d, J = 1.4 Hz, $CH{=}CH_{Im}$), 10.48 (t, J = 1.6 Hz, 1H, NCHN).

$^{13}C\{^1H\}$-NMR ($CDCl_3$, T = 298 K, ppm) δ: 18.0 (CH_3, *o*-$CH_{3(IMes)}$), 21.3 (CH_3, *p*-$CH_{3(IMes)}$), 61.0 (CH_2, allyl-CH_2), 109.6 (CH, allyl-CH), 124.1 (CH, $CH{=}CH_{Im}$), 129.9 (CH, *m*-$CH_{(IMes)}$), 131.1 (C, *o*-$C_{(IMes)}$), 134.7 (CH, *p*-$CH_{(IMes)}$), 140.2 (CH, NCHN), 141.2 (C, *i*-$C_{(IMes)}$).

Elemental analysis calcd (%) for $C_{24}H_{30}Cl_2N_2Pd$: C, 55.03, H, 5.77, N, 5.35; found: C, 55.39, H, 5.60, N, 5.28.

Synthesis of [SIPr·H][PdCl$_2$(allyl)] (2c)

Following the general procedure from SIPr·HCl (66.4 mg, 0.156 mmol) and $[Pd(allyl)(\mu\text{-}Cl)]_2$ (28.5 mg, 0.0779 mmol), the product was obtained as a pale-yellow powder in a quantitative yield.

^1H-NMR (400 MHz, $CDCl_3$, T = 298 K, ppm) δ: 1.22 (d, J = 6.9 Hz, 12H, $CH_{3(SIPr)}$), 1.42 (d, J = 6.9 Hz, 12H, $CH_{3(SIPr)}$), 2.86 (d, J = 12.0 Hz, 2H, *anti* allyl-H), 3.17 (hept, J = 6.9 Hz, 4H, $C\underline{H}(CH_3)_2$), 3.93 (d, J = 6.7 Hz,

2H, *syn* allyl-H), 5.03 (s, 4H, CH_2–CH_2), 5.30 (m, 1H, *central* allyl-H), 7.28 (d, $J=7.7$ Hz, 4H, *m*-$H_{(SIPr)}$), 7.46 (t, $J=7.7$ Hz, 2H, *p*-$H_{(IPr)}$), 7.54 (s, 1H, NCHN).

Elemental analysis calcd (%) for $C_{30}H_{44}Cl_2N_2Pd$: C, 59.07, H, 7.27, N, 4.59; found: C, 59.38, H, 7.20, N, 4.69.

Synthesis of [SIMes·H][PdCl$_2$(allyl)] (2 d)

Following the general procedure from SIMes·HCl (55.1 mg, 0.161 mmol) and $[Pd(allyl)(\mu\text{-}Cl)]_2$ (29.4 mg, 0.0803 mmol), the product was obtained as a pale-yellow powder in a quantitative yield.

^{1}H-NMR (400 MHz, $CDCl_3$, T = 298 K, ppm) δ: 2.27 (s, 6H, *p*-$CH_{3(SIMes)}$), 2.39 (s, 12H, *o*-$CH_{3(SIMes)}$), 2.56 (d, $J=12.0$ Hz, 2H, *anti* allyl-H), 3.75 (d, $J=6.7$ Hz, 2H, *syn* allyl-H), 4.54 (s, 4H, CH_2–CH_2), 5.10 (m, 1H, *central* allyl-H), 6.91 (s, 4H, *m*-$H_{(SIMes)}$), 9.00 (bs, 1H, NCHN).

^{13}C{^{1}H}-NMR ($CDCl_3$, T = 298 K, ppm) δ: 18.3 (CH_3, *o*-$CH_{3(SIMes)}$), 21.1 (CH_3, *p*-$CH_{3(SIMes)}$), 52.2 (CH_2, CH_2–CH_2), 60.9 (CH_2, allyl-CH_2), 109.5 (CH, allyl-CH), 130.0 (CH, *m*-$CH_{(SIMes)}$), 130.7 (C, *o*-$C_{(SIMes)}$), 135.5 (CH, *p*-$CH_{(SIMes)}$), 140.4 (C, *i*-$C_{(SIMes)}$), 159.8 (CH, NCHN).

Elemental analysis calcd (%) for $C_{24}H_{32}Cl_2N_2Pd$: C, 54.82, H, 6.13, N, 5.33; found: C, 55.09, H, 6.02, N, 5.24.

Synthesis of [IPr^{Cl}·H][PdCl$_2$(allyl)] (2 e)

Following the general procedure from IPr^{Cl}·HCl (79.9 mg, 0.162 mmol) and $[Pd(allyl)(\mu\text{-}Cl)]_2$ (29.6 mg, 0.0809 mmol), the product was obtained as a pale-yellow powder in a quantitative yield.

^{1}H-NMR (400 MHz, $CDCl_3$, T = 298 K, ppm) δ: 1.27 (d, $J=6.8$ Hz, 12H, $CH_{3(IPrCl)}$), 1.40 (d, $J=6.8$ Hz, 12H, $CH_{3(IPrCl)}$), 2.38 (hept, $J=6.8$ Hz, 4H, C<u>H</u>$(CH_3)_2$), 2.70 (d, $J=12.1$ Hz, 2H, *anti* allyl-H), 3.80 (d, $J=6.4$ Hz, 2H, *syn* allyl-H), 5.17 (m, 1H, *central* allyl-H), 7.38 (d, $J=7.8$ Hz, 4H, *m*-$H_{(IPrCl)}$), 7.61 (t, $J=7.8$ Hz, 2H, *p*-$H_{(IPrCl)}$), 12.19 (bs, 1H, NCHN).

Elemental analysis calcd (%) for $C_{30}H_{40}Cl_4N_2Pd$: C, 53.23, H, 5.96, N, 4.14; found: C, 53.01, H, 6.14, N, 4.26.

Synthesis of [IPr·H][PdCl$_2$(allyl)] (2 f)*

Following the general procedure from IPr*·HCl (95.0 mg, 0.100 mmol) and $[Pd(allyl)(\mu\text{-}Cl)]_2$ (18.3 mg, 0.0500 mmol), the product was obtained as a pale-yellow powder in a quantitative yield.

^{1}H-NMR (300 MHz, $CDCl_3$, T = 298 K, ppm) δ: 2.17 (s, 6H, $CH_{3(IPr*)}$), 2.71 (d, $J=11.9$ Hz, 2H, *anti* allyl-H), 3.88 (d, $J=6.3$ Hz, 2H, *syn* allyl-H), 5.16 (m, 1H, *central* allyl-H), 5.26 (d, $J=1.5$ Hz, 2H, CH=CH_{Im}), 5.49 (s, 4H, <u>CH</u>-Ph_2), 6.72–7.38 (m, 40H, Ar-$H_{(IPr*)}$), 12.23 (s, 1H, NCHN).

^{13}C{^{1}H}-NMR ($CDCl_3$, T = 298 K, ppm) δ: 22.0 (CH_3, $CH_{3(IPr*)}$), 51.2 (CH, <u>CH</u>-Ph_2), 61.0 (CH_2, allyl-CH_2), 109.5 (CH, allyl-CH), 123.0 (CH, CH=CH_{Im}), 126.8–142.9 (Ar-$C_{(IPr*)}$), 142.4 (CH, NCHN).

Elemental analysis calcd (%) for $C_{72}H_{62}Cl_2N_2Pd$: C, 76.35, H, 5.52, N, 2.47; found: C, 76.60, H, 5.41, N, 2.39.

Synthesis of [IPr·H][PdCl$_2$(indenyl)] (3 a)

Following the general procedure from IPr·HCl (115.6 mg, 0.2723 mmol) and $[Pd(indenyl)(\mu\text{-}Cl)]_2$ (70.0 mg, 0.1362 mmol), the product was obtained as a brownish powder in a quantitative yield.

^{1}H-NMR (400 MHz, $CDCl_3$, T = 298 K, ppm) δ: 1.20 (d, $J=6.8$ Hz, 12H, $CH_{3(IPr)}$), 1.28 (d, $J=6.8$ Hz, 12H, $CH_{3(IPr)}$), 2.48 (hept, $J=6.8$ Hz, 4H, C<u>H</u>$(CH_3)_2$), 5.65 (bs, 2H, H^1, H^3 indenyl), 6.57–6.59 (m, 2H, H^4, H^7 indenyl), 6.81–6.83 (m, 2H, H^5, H^6 indenyl), 6.86 (bs, 1H, H^2 indenyl), 7.34 (d, $J=7.8$ Hz, 4H, *m*-$H_{(IPr)}$), 7.57 (t, $J=7.8$ Hz, 2H, *p*-$H_{(IPr)}$) 8.20 (d, $J=1.7$ Hz, 2H, CH=CH_{Im}), 9.04 (t, $J=1.7$ Hz, 1H, NCHN).

^{13}C{^{1}H}-NMR ($CDCl_3$, T = 298 K, ppm) δ: 24.1 (CH_3, $CH_{3(IPr)}$), 24.8 (CH_3, $CH_{3(IPr)}$), 29.2 (CH, <u>CH</u>$(CH_3)_2$), 76.2 (CH, CH^1, CH^3 indenyl), 109.8 (CH, CH^2 indenyl), 117.8 (CH, CH^5, CH^6 indenyl), 124.8 (CH, *m*-$CH_{(IPr)}$), 125.8 (CH, CH^4, CH^7 indenyl), 127.7 (CH, CH=CH_{Im}), 130.1 (C, *o*-$C_{(IPr)}$), 132.2 (C, *p*-$C_{(IPr)}$), 136.8 (CH, NCHN), 141.7 (C, C^{3a}, C^{7a} indenyl), 145.3 (CH, *i*-$CH_{(IPr)}$).

Elemental analysis calcd (%) for $C_{36}H_{44}Cl_2N_2Pd$: C, 63.39, H, 6.50, N, 4.11; found: C, 63.02, H, 6.68, N, 4.04.

Synthesis of [IMes·H][PdCl$_2$(indenyl)] (3 b)

Following the general procedure from IMes·HCl (66.8 mg, 0.1969 mmol) and $[Pd(indenyl)(\mu\text{-}Cl)]_2$ (50.4 mg, 0.0980 mmol), the product was obtained as a brownish powder in a quantitative yield.

^{1}H-NMR (400 MHz, $CDCl_3$, T = 298 K, ppm) δ: 2.17 (s, 12H, *o*-$CH_{3(IMes)}$), 2.36 (s, 6H, *p*-$CH_{3(IMes)}$), 5.58 (d, $J=3.1$ Hz, 2H, H^1, H^3 indenyl), 6.59 (dd, $J=3.1$, 5.3 Hz, 2H, H^4, H^7 indenyl), 6.60 (t, $J=3.1$ Hz, 1H, H^2 indenyl) 6.59 (dd, $J=3.1$, 5.3 Hz, 2H, H^5, H^6 indenyl), 7.03 (s, 4H, *m*-$H_{(IMes)}$), 7.58 (d, $J=1.6$ Hz, CH=CH_{Im}), 10.12 (t, $J=1.6$ Hz, 1H, NCHN).

^{13}C{^{1}H}-NMR ($CDCl_3$, T = 298 K, ppm) δ: 17.9 (CH_3, *o*-$CH_{3(IMes)}$), 21.3 (CH_3, *p*-$CH_{3(IMes)}$), 73.2 (CH, CH^1, CH^3 indenyl), 109.6 (CH, CH^2 indenyl), 117.8 (CH, CH^5, CH^6 indenyl), 124.7 (CH, CH=CH_{Im}), 125.8 (CH, CH^4, CH^7 indenyl), 130.0 (CH, *m*-$CH_{(IMes)}$), 130.9 (C, *o*-$C_{(IMes)}$), 134.4 (C, *p*-$C_{(IMes)}$), 139.2 (CH, NCHN), 141.4 (C, *i*-$C_{(IMes)}$), 141.6 (C, C^{3a}, C^{7a} indenyl).

Elemental analysis calcd (%) for $C_{30}H_{32}Cl_2N_2Pd$: C, 60.26, H, 5.39, N, 4.69; found: C, 60.04, H, 5.50, N, 4.57.

Synthesis of [SIPr·H][PdCl$_2$(indenyl)] (3 c)

Following the general procedure from SIPr·HCl (116.5 mg, 0.2727 mmol) and $[Pd(indenyl)(\mu\text{-}Cl)]_2$ (70.1 mg, 0.1363 mmol), the product was obtained as a brownish powder in a quantitative yield.

^{1}H-NMR (400 MHz, $CDCl_3$, T = 298 K, ppm) δ: 1.21 (d, $J=6.9$ Hz, 12H, $CH_{3(SIPr)}$), 1.40 (d, $J=6.9$ Hz, 12H, $CH_{3(SIPr)}$), 3.07 (hept, $J=6.9$ Hz, 4H, C<u>H</u>$(CH_3)_2$), 4.88 (s, 4H, CH_2-CH_2), 5.69 (d, $J=3.1$ Hz, 2H, H^1, H^3 indenyl), 6.43 (dd, $J=3.1$, 5.3 Hz, 2H, H^4, H^7 indenyl), 6.77 (dd, $J=3.1$, 5.3 Hz, 2H, H^5, H^6 indenyl), 6.91 (t, $J=3.1$ Hz, 1H, H^2 indenyl), 7.27 (d, $J=7.8$ Hz, 4H, *m*-$H_{(SIPr)}$), 7.46 (t, $J=7.8$ Hz, 2H, *p*-$H_{(SIPr)}$), 7.71 (s, 1H, NCHN).

Elemental analysis calcd (%) for $C_{36}H_{46}Cl_2N_2Pd$: C, 63.21, H, 6.78, N, 4.10; found: C, 63.47, H, 6.60, N, 4.23.

Synthesis of [SIMes·H][PdCl$_2$(indenyl)] (3 d)

Following the general procedure from SIMes·HCl (93.6 mg, 0.2739 mmol) and $[Pd(indenyl)(\mu\text{-}Cl)]_2$ (70.4 mg, 0.1369 mmol), the product was obtained as a brownish powder in a quantitative yield.

^{1}H-NMR (400 MHz, $CDCl_3$, T = 298 K, ppm) δ: 2.32 (s, 6H, *p*-$CH_{3(SIMes)}$), 2.35 (s, 12H, *o*-$CH_{3(SIMes)}$), 4.62 (s, 4H, CH_2–CH_2), 5.70 (bs, 2H, H^1, H^3 indenyl) 6.45 (bs, 1H, H^2 indenyl) 6.79–7.83 (4H, H^4, H^5, H^6, H^7 indenyl), 6.97 (s, 4H, *m*-$H_{(SIMes)}$), 8.02 (bs, 1H, NCHN).

^{13}C{^{1}H}-NMR ($CDCl_3$, T = 298 K, ppm) δ: 18.2 (CH_3, *o*-$CH_{3(SIMes)}$), 21.2 (CH_3, *p*-$CH_{3(SIMes)}$), 52.7 (CH_2, CH_2–CH_2), 77.4 (CH, CH^1, CH^3 indenyl), 110.0 (CH, CH^2 indenyl), 118.0 (CH, CH^5, CH^6 indenyl), 126.0 (CH,

CH[4], CH[7] indenyl), 130.2 (CH, *m*-$CH_{(SIMes)}$), 130.5 (C, *o*-$C_{(SIMes)}$), 135.4 (C, *p*-$C_{(SIMes)}$), 140.7 (C, *i*-$C_{(SIMes)}$), 141.3 (C, C^{3a}, C^{7a} indenyl), 158.3 (CH, NCHN).

Elemental analysis calcd (%) for $C_{30}H_{34}Cl_2N_2Pd$: C, 60.06, H, 5.71, N, 4.67; found: C, 60.29, H, 5.65, N, 4.57.

Synthesis of [IPr^{Cl}·H][PdCl$_2$(indenyl)] (3 e)

Following the general procedure from IPr^{Cl}·HCl (116.5 mg, 0.2349 mmol) and [Pd(indenyl)(μ-Cl)]$_2$ (60.4 mg, 0.1174 mmol), the product was obtained as a brownish powder in a quantitative yield.

^{1}H-NMR (400 MHz, $CDCl_3$, T = 298 K, ppm) δ: 1.26 (d, *J* = 6.8 Hz, 12H, $CH_{3(IPrCl)}$), 1.34 (d, *J* = 6.8 Hz, 12H, $CH_{3(IPrCl)}$), 2.34 (hept, *J* = 6.9 Hz, 4H, C<u>H</u>$(CH_3)_2$), 5.44 (bs, 2H, H^1, H^3 indenyl), 6.58–6.73 (m, 5H, H^2, H^4, H^5, CH^6, H^7 indenyl), 7.36 (d, *J* = 7.8 Hz, 4H, *m*-$H_{(IPrCl)}$), 7.63 (t, *J* = 7.8 Hz, 2H, *p*-$H_{(IPrCl)}$), 12.20 (bs, 1H, NCHN).

Elemental analysis calcd (%) for $C_{36}H_{42}Cl_4N_2Pd$: C, 57.58, H, 5.64, N, 3.73; found: C, 57.90, H, 5.51, N, 3.65.

Synthesis of [IPr·H][PdCl$_2$(indenyl)] (3 f)*

Following the general procedure from IPr*·HCl (148.5 mg, 0.1564 mmol) and [Pd(indenyl)(μ-Cl)]$_2$ (40.2 mg, 0.0782 mmol), the product was obtained as a brownish powder in a quantitative yield.

^{1}H-NMR (300 MHz, $CDCl_3$, T = 298 K, ppm) δ: 2.18 (s, 6H, $CH_{3(IPr*)}$), 5.35 (d, *J* = 1.5 Hz, 2H, CH=CH_{Im}), 5.39 (s, 4H, <u>CH</u>-Ph_2), 5.68 (bs, 2H, H^1, H^3 indenyl), 6.60–7.25 (m, 45H, Ar-$H_{(IPr*)}$, H^2, H^4, H^5, H^6, H^7 indenyl), 12.18 (s, 1H, NCHN).

^{13}C{^{1}H}-NMR ($CDCl_3$, T = 298 K, ppm) δ: 22.0 (CH_3, $CH_{3(IPr*)}$), 51.2 (CH, <u>CH</u>-Ph_2), 76.0 (CH, CH^1, CH^3 indenyl), 109.7 (CH, CH^2 indenyl), 118.3 (CH, CH^5, CH^6 indenyl), 123.1 (CH, CH=CH_{Im}), 126.1–142.7 (Ar-$C_{(IPr*)}$, CH, CH^4, CH^7 indenyl), 141.8 (CH, NCHN), 142.1 (C, C^{3a}, C^{7a} indenyl).

Elemental analysis calcd (%) for $C_{78}H_{64}Cl_2N_2Pd$: C, 77.64, H, 5.35, N, 2.32; found: C, 77.96, H, 5.22, N, 2.25.

Synthesis of [Pd(IPr)(PTA)(allyl)]BF$_4$ (5 a)

In a 50 mL round-bottom flask, 197.4 mg of [Pd(IPr)Cl(allyl)] **4 a** (0.345 mmol) was dissolved in 1 mL of technical grade acetone.

A solution of 1,3,5-triaza-7-phosphaadamantane (54.2 mg, 0.345 mmol) and $NaBF_4$ (37.9 mg, 0.345 mmol) in 20 mL of technical grade acetone was added to the solution containing the palladium precursor. The reaction mixture was stirred for 15 min at room temperature and then the NaCl was removed by filtration on a millipore membrane filter. Addition of pentane to the concentrated solution yields the precipitation of the final complex as a white solid, which was filtered and dried under vacuum.

245.1 mg was obtained (91 % yield).

^{1}H NMR ($CDCl_3$, T = 298 K, ppm): δ (ppm) = 7.54 (t, *J* = 7.8 Hz, 2 H, $H_{Ar(IPr)}$), 7.49 (s, 2 H, H_{Imid}), 7.35–7.42 (m, 4 H, $H_{Ar(IPr)}$), 4.95–5.09 (m, 1H, *central* allyl-H), 4.36–4.38 (m, 7H, PCH_2N, *syn* allyl-H trans-P), 3.80–3.83 (m, 1H, *syn* allyl-H trans-C), 3.56–3.80 (m, 6H, NCH2 N), 2.97 (hept, *J* = 6.8 Hz, 2 H, $CH(CH_3)_{2(IPr)}$), 2.77 (hept, *J* = 6.7 Hz, 2 H, $CH(CH_3)_{2(IPr)}$), 2.29 (d, 1H, J_{HH} = 13.1 Hz, anti allyl-H trans-C), 1.92 (dd, J_{HH} = 13.7 Hz, J_{HP} = 9.6 Hz, 1H, anti allyl-H trans-P), 1.38 (d, *J* = 6.7 Hz, 6 H, $CH(CH_3)_{2(IPr)}$), 1.28 (d, *J* = 6.8 Hz, 6 H, $CH(CH_3)_{2(IPr)}$), 1.26 (d, *J* = 6.7 Hz, 6 H, $CH(CH_3)_{2(IPr)}$), 1.07 ppm (d, *J* = 6.8 Hz, 6 H, $(CH_3)_{2(IPr)}$).

^{31}P{^{1}H} NMR ($CDCl_3$, T = 298 K, ppm) δ: −57.4.

^{19}F{^{1}H} NMR ($CDCl_3$, T = 298 K, ppm) δ: −152.5 ($^{10}BF_4$), −152.6 ($^{11}BF_4$).

^{13}C {^{1}H} NMR ($CDCl_3$, T = 298 K, ppm): δ (ppm) = 181.5 (d, C, J_{CP} = 15.7 Hz, carbene), 135.4 (C, $C_{Ar(IPr)}$), 130.9 (CH, $CH_{Ar(IPr)}$), 125.4 (CH, CH_{Im}), 125.1 (CH, $CH_{Ar(IPr)}$), 125.0 (CH, $CH_{Ar(IPr)}$), 124.8 (CH, CH_{Im}), 120.9 (d, CH, J_{CP} = 5.0 Hz, central allyl), 72.8 (d, CH_2, J_{CP} = 7.2 Hz, NCH_2N), 71.6 (d, CH_2, J_{CP} = 28.1 Hz, allyl trans-P), 62.5 (CH_2, allyl trans-C), 51.9 (d, CH_2, J_{CP} = 12.0 Hz, NCH_2P), 29.1 (<u>CH</u>$(CH_3)_{2(IPr)}$), 28.9 (<u>CH</u>$(CH_3)_{2(IPr)}$), 27.5 (CH_{3IPr}), 26.0 (CH_{3IPr}), 22.8 (CH_{3IPr}), 22.6 (CH_{3IPr}).

Elemental analysis calcd (%) for $C_{36}H_{53}BF_4N_5PPd$: C, 55.43, H, 6.85, N, 8.98; found: C, 55.19, H, 6.98, N, 9.10.

Synthesis of [Pd(IMes)(PTA)(allyl)]BF$_4$ (5 b)

In a 50 mL round-bottom flask, 149.9 mg of [Pd(IMes)Cl(allyl)] **4 b** (0.308 mmol) was dissolved in 1 mL of technical grade acetone.

A solution of 1,3,5-triaza-7-phosphaadamantane (48.3 mg, 0.308 mmol) and $NaBF_4$ (33.8 mg, 0.308 mmol) in 20 mL of technical grade acetone was added to the solution containing the palladium precursor. The reaction mixture was stirred for 15 min at room temperature and then the NaCl was removed by filtration on a millipore membrane filter. Addition of pentane to the concentrated solution yields the precipitation of the final complex as a white solid, which was filtered and dried under vacuum.

212.4 mg was obtained (99 % yield).

^{1}H NMR (CD_3CN, T = 298 K, ppm): δ (ppm) = 7.49 (s, 2H, H_{Imid}), 7.14 (s, 2H, $H_{Ar(IMes)}$), 7.08 (s, 2H, $H_{Ar(IMes)}$), 4.89–5.02 (m, 1H, *central* allyl-H), 4.30–4.40 (m, 6H, PCH_2N), 4.04–4.09 (m, 1H, *syn* allyl-H trans-P), 3.85 (d, 1H, J_{HH} = 7.4 Hz, *syn* allyl-H trans-C), 3.55–3.79 (m, 6H, NCH_2N), 2.33 (s, 6 H, p-mesityl-CH_3), 2.30 (d, 1H, J_{HH} = 13.3 Hz, anti allyl-H trans-C), 2.18 (s, 6 H, o-mesityl-CH_3), 2.08 (s, 6 H, o-mesityl-CH_3), 2.01–2.06 (m, 1H, anti allyl-H trans-P).

^{31}P{^{1}H} NMR (CD_3CN, T = 298 K, ppm) δ: −59.5.

^{19}F{^{1}H} NMR (CD_3CN, T = 298 K, ppm) δ: −151.8 ($^{10}BF_4$), −151.9 ($^{11}BF_4$).

^{13}C {^{1}H} NMR (CD_3CN, T = 298 K, ppm): δ (ppm) = 179.4 (d, C, J_{CP} = 16.3 Hz, carbene), 140.6 (C, $C_{Ar(IMes)}$), 136.6 (C, $C_{Ar(IMes)}$), 136.2 (C, $C_{Ar(IMes)}$), 135.6 (C, $C_{Ar(IMes)}$), 130.7 (CH, $CH_{Ar(IMes)}$), 130.5 (CH, $CH_{Ar(IMes)}$), 125.9 (CH, CH_{Im}), 121.6 (d, CH, J_{CP} = 4.8 Hz, central allyl), 73.2 (d, CH_2, J_{CP} = 7.3 Hz, NCH_2N), 72.3 (d, CH_2, J_{CP} = 27.7 Hz, allyl trans-P), 61.5 (CH_2, allyl trans-C), 52.9 (d, CH_2, J_{CP} = 11.8 Hz, NCH_2P), 21.0 (CH_3, p-mesityl-CH_3), 19.3 (CH_3, o-mesityl-CH_3), 19.2 (CH_3, o-mesityl-CH_3).

Elemental analysis calcd (%) for $C_{30}H_{41}BF_4N_5PPd$: C, 51.78, H, 5.94, N, 10.06; found: C, 51.50, H, 6.11, N, 10.19.

Computational Details

Density Functional Theory (DFT) calculations were carried out with the Amsterdam Density Functional (ADF) software,[28–30] using the BLYP[31] functional and employing the zeroth-order regular approximation (ZORA)[32] to take into account scalar relativistic effects, which are mandatory in the presence of heavy nuclei.[33] Grimme dispersion correction was included.[34,35] The TZ2P basis set was used for all the elements. It is a large, uncontracted set of Slater-type orbitals (STOs), is of triple-ζ quality and is augmented with two sets of polarization functions on each atom. In addition, core electrons were described with the frozen-core approximation: up to 1 s for C, N, O and Cl, and up to 3d in the case of Pd; the level of theory is denoted in the text ZORA-BLYP-D3(BJ)/TZ2P. For the numerical integration, the Becke grid was used.[36] Frequency calculations were run to assess the nature of the structures located

on the potential energy surface: all minima have real frequencies. To gain quantitative insight into the stability of the compounds, we performed an activation strain (ASA) and energy decomposition analysis (EDA)[37,38] as implemented in ADF. Using this fragment-based approach, according to the ASA scheme, we have decomposed the energy relative to the reactants into *strain*, ΔE_{strain} (*i.e.* the deformation energy required by the reactants to acquire the structure they have in the compound of interest) and *interaction*, ΔE_{int} (*i.e.* the interaction energy between the deformed reactants) (Eq. 1):

$$\Delta E_{=}\Delta E_{strain} + \Delta E_{int} \quad (1)$$

Within EDA, ΔE_{int} can be written as the sum of *electrostatic interaction* (ΔV_{elstat}), the interaction between Coulomb charge densities, *Pauli repulsion* (ΔE_{Pauli}), related to the repulsive interaction between filled orbitals, *orbital interaction* (ΔE_{oi}) due to stabilizing interactions such as HOMO-LUMO interaction (Eq. 2) and *dispersion interaction* (ΔE_{disp}):

$$\Delta E_{int=}\Delta V_{elstat} + \Delta E_{Pauli} + \Delta E_{oi} + \Delta E_{disp} \quad (2)$$

The Voronoi deformation density (VDD) method for the calculation of atomic charges was used to analyze the electron density distribution.[39] The VDD charge on atom A (Q_A^{VDD}) is the integral of the deformation density in the volume of the Voronoi cell of atom A:

$$Q_A^{VDD} = -\int_{Voronoi\ cell\ of\ atom\ A}\left[\rho(r) - \sum_B \rho_B(r)\right]dr \quad (3)$$

$\rho(r)$ is the electron density of the molecule and $\sum_B \rho_B(r)$ is the sum of the electron densities of a fictitious molecule in which all atoms are considered non-interacting and neutral. The physical meaning is clear: Q_A^{VDD} is not a charge associated to atom A, but it is a measure of the amount of charge flowing into ($Q_A^{VDD} < 0$) or out ($Q_A^{VDD} > 0$) the Voronoi cell of atom A due to chemical interactions. The VDD scheme can be extended to study chemical bonding between fragments. In our case, we have defined:

$$\Delta Q_A^{VDD} = \int_{Voronoi\ cell\ of\ atom\ A\ in\ the\ complex}\left[\rho_{complex}(r) - \rho_{Fragment1}(r) - \rho_{Fragment2}(r)\right]dr \quad (4)$$

Solvent effects were treated with the Conductor-like Screening Model (COSMO),[40] which is implemented in the ADF program. For chloroform, DMSO and water, we used a solvent-excluding surface with an effective radius of 3.17 Å, 3.04 Å and 1.93 Å, and a relative dielectric constant of 4.8, 46.7 and 78.39, respectively. The empirical parameter in the scaling function in the COSMO equation was set to 0.0. The radii of the atoms were taken to be MM3 radii,[41] divided by 1.2, giving 1.350 Å for H, 1.700 Å for C, 1.608 for N, 1.725 Å for Cl and 1.975 Å for Pd.[42] The geometries of **2a** and **3a** and those of the separated fragments were fully reoptimized in solvent (level of theory: COSMO-ZORA-BLYP-D3(BJ)/TZ2P).

Cell Viability Assay

Cells were grown in agreement with the supplier and incubated at 37 °C (5% of CO_2). 500 cells were plated in 96 wells and treated with six different concentrations of carbene-metal-amido complexes (0.001, 0.01, 0.1, 1, 10, and 100 μM). After 96 hours, cell viability was evaluated with CellTiter glow assay (Promega, Madison, WI, USA) with a Tecan M1000 instrument. IC_{50} values were obtained from triplicates, and error bars are standard deviations.

With a similar procedure, organoids were plated as single cells as possible (around 1000 cells) in five replicates and treated with six serial dilutions of the compounds (0.001, 0.01, 0.1, 1, 10, and 100 μM) and analyzed after 96 h.

Bacterial Thioredoxin Reductase Activity Assay

The DTNB-coupled thioredoxin reductase activity assay based on Lu et al.[43] was established and modified for our purposes by Schmidt et al.[24a] All reagents and solvents were purchase from Sigma Aldrich (Germany) if not stated differently. Thioredoxin reductase (TrxR) from *E. coli* (CAS: 9074–14-0) and the substrate thioredoxin (Trx) from *E. coli* recombinant was purchased (CAS: 52500–60-4). Stock solutions were prepared by dilution with TE buffer to achieve a concentration of 35.5 U/mL for the enzyme and 6.1 U/mL for the substrate. For TE buffer (pH 7.5) preparation, Tris-HCl (final concentration: 50 mM) and EDTA (final: concentration: 1 mM) were dissolved in ultrapure water, and pH was adjusted with 1 M NaOH. The palladium compounds were freshly dissolved in DMF (stock solution) in a 200-times higher concentration than the highest test concentration used for these studies and diluted with TE buffer (final DMF concentration: 0.5%).

Aliquots of the TrxR enzyme solution (10 μL), Trx substrate solution (10 μL), and NADPH (200 mM) in TE buffer (100 μL) were mixed in a well either containing the compounds (20 μL) in graded concentrations or only DMF in buffer (positive control). The resulting solutions were incubated with moderate shaking for 75 min at 25 °C in a 96-well plate. Afterward, 100 μL of the reaction mixture (containing 200 mM NADPH and 5 mM DTNB in TE buffer solution) was added to each well. Thereby the conversion of DTNB to 5-TNB was initiated and monitored with a microplate reader (Tecan infinite M nano +) at 412 nm, ten times in 35-sec intervals for about 6 min.

The values were corrected using the absorbance of the blank solution. The increase in 5-TNB concentration over time followed a linear trend ($r^2 \geq 0.990$), and the enzymatic activities were calculated as the slopes (increase in absorbance per second) thereof. For each tested compound, non-interference with the assay components was confirmed by a negative control experiment. The highest test compound concentration was used, and the aliquot of enzyme solution was replaced by the same amount of TE buffer. IC_{50} values were calculated as the concentration of the compound decreasing the enzymatic activity of the positive control by 50% and are given as the means and error of three repeated experiments.

Crystal Structure Determination

3b and **2f** crystals data were collected at 100 K at the XRD2 beamline of the Elettra Synchrotron, Trieste (Italy),[44] using a monochromatic wavelength of 0.620 Å. The data sets were integrated, scaled and corrected for Lorentz, absorption and polarization effects using XDS package.[45] The structures were solved by direct methods using SHELXT program[46] and refined using full-matrix least-squares implemented in SHELXL-2018/3.[47] Thermal motions for all non-hydrogen atoms have been treated anisotropically and hydrogens have been included on calculated positions, riding on their carrier atoms. Geometric restrains (SAME) have been applied to disordered allyl fragment and solvent in 1f. Coot program was used for model building.[48] The crystal data are

given in Table S10. Pictures were prepared using Ortep3[49] and Pymol[50] software.

Deposition Numbers 2150853 (for **3 b**) and 2150854 (for **2 f**) contain the supplementary crystallographic data for this paper. These data are provided free of charge by the joint Cambridge Crystallographic Data Centre and Fachinformationszentrum Karlsruhe Access Structures service www.ccdc.cam.ac.uk/structures.

Acknowledgements

We are grateful to the SBO (D2 M to SPN) and the BOF (starting and senior grants to SPN) as well as the iBOF C3 project for financial support. FR was financially supported by Fondazione AIRC per la Ricerca sul Cancro (Grant AIRC IG23566) and VC from Ministero della Salute – Ricerca Corrente. Calculations were carried out using cloud facilities provided by CINECA (ISCRA C project HP10CAQKAM PROSIT). Open Access Funding provided by Universita degli Studi di Padova within the CRUI-CARE Agreement.

Conflict of Interest

The authors declare no conflict of interest.

Data Availability Statement

The data that support the findings of this study are available in the supplementary material of this article.

Keywords: Allyl and indenyl palladium complexes · Anticancer activity · Mechanochemistry · *N*-heterocyclic carbenes · Thioredoxin reductase inhibition

[1] a) R. A. Alderden, M. D. Hall, T. W. Hambley, *J. Chem. Educ.* **2006**, *83*, 728–734; b) D. Wang, S. J. Lippard, *Nat. Rev. Drug Discovery* **2005**, *4*, 307–320.
[2] L. R. Kelland, N. P. Farrell, *Platinum-Based Drugs in Cancer Therapy*, Humana Press Inc., Totowa, NJ, **2000**.
[3] a) R. Oun, Y. E. Moussa, N. J. Wheate, *Dalton Trans.* **2018**, *47*, 6645–6653; b) L. Kelland, *Nat. Rev. Cancer* **2007**, *7*, 573–584.
[4] a) C. A. Almeida, S. A. Barry, *Cancer: Basic Science and Clinical Aspects*, Wiley-Blackwell, Chichester, **2010**; b) E. Alessio, *Bioinorganic Medicinal Chemistry*, Wiley-VCH, Weinheim, **2011**; c) I. Ott, *Adv. Inorg. Chem.* **2020**, *75*, 121–148; d) S. Y. Lee, C. Y. Kim, T.-G. Nam, *Drug Des. Dev. Ther.* **2020**, *14*, 5375–5392; e) E. J. Anthony, E. M. Bolitho, H. E. Bridgewater, O. W. L. Carter, J. M. Donnelly, C. Imberti, E. C. Lant, F. Lermyte, R. J. Needham, M. Palau, P. J. Sadler, H. Shi, F.-X. Wang, W.-Y. Zhang, Z. Zhang, *Chem. Sci.* **2020**, *11*, 12888–12917; f) P. Zhang, P. J. Sadler, *J. Organomet. Chem.* **2017**, *839*, 5–14; g) S. Jürgens, F. E. Kühn, A. Casini, *Curr. Med. Chem.* **2017**, *25*, 437–461; h) J. C. Páez-Franco, M. R. Zermeño-Ortega, C. M. de la O-Contreras, D. Canseco-González, J. R. Parra-Unda, A. Avila-Sorrosa, R. G. Enríquez, J. M. Germán-Acacio, D. Morales-Morales, *Pharmaceutica* **2022**, *14*, 402; i) D. Hernández-Romero, S. Rosete-Luna, A. López-Monteon, A. Chávez-Piña, N. Pérez-Hernández, J. Marroquín-Flores, A. Cruz-Navarro, G. Pesado-Gómez, D. Morales-Morales, R. Colorado-Peralta, *Coord. Chem. Rev.* **2021**, *439*, 213930.
[5] a) M. Mora, M. C. Gimeno, R. Visbal, *Chem. Soc. Rev.* **2019**, *48*, 447–462; b) T. A. C. A. Bayrakdar, T. Scattolin, X. Ma, S. P. Nolan, *Chem. Soc. Rev.* **2020**, *49*, 7044–7100; c) B. Bertrand, A. Casini, *Dalton Trans.* **2014**, *3*, 4209–4219; d) S. Nobili, E. Mini, I. Landini, C. Gabbiani, A. Casini, L. Messori, *Med. Res. Rev.* **2010**, *30*, 550–80.
[6] a) S. Y. Lee, C. Y. Kim, T.-G. Nam, *Drug Des. Dev. Ther.* **2020**, *14*, 5375–5392; b) S. Q. Zhang, L.-H. Gao, H. Zhao, K.-Z. Wang, *Curr. Med. Chem.* **2020**, *27*, 3735–3752.
[7] a) T. Scattolin, V. A. Voloshkin, F. Visentin, S. P. Nolan, *Cell Rep.* **2021**, *2*, 100446; b) A. R. Kapdi, I. J. Fairlamb, *Chem. Soc. Rev.* **2014**, *43*, 4751; c) T. Scattolin, S. Giust, P. Bergamini, I. Caligiuri, L. Canovese, N. Demitri, R. Gambari, I. Lampronti, F. Rizzolio, F. Visentin, *Appl. Organomet. Chem.* **2019**, *33*, e4902; d) T. Scattolin, I. Caligiuri, N. Mouawad, M. El Boustani, N. Demitri, F. Rizzolio, F. Visentin, *Eur. J. Med. Chem.* **2019**, *179*, 325–334; e) S. J. Sabounchei, M. Sayadi, A. Hashemi, S. Salehzadeh, F. Maleki, D. Nematollahi, B. Mokhtari, L. Hosseinzadeh, *J. Organomet. Chem.* **2018**, *860*, 49–58; f) T. Scattolin, N. Pangerc, I. Lampronti, C. Tupini, R. Gambari, L. Marvelli, F. Rizzolio, N. Demitri, L. Canovese, F. Visentin, *J. Organomet. Chem.* **2019**, *899*, 120857.
[8] a) T. Scattolin, E. Bortolamiol, F. Visentin, S. Palazzolo, I. Caligiuri, T. Perin, V. Canzonieri, N. Demitri, F. Rizzolio, A. Togni, *Chem. Eur. J.* **2020**, *26*, 11868–11876; b) T. Scattolin, I. Caligiuri, L. Canovese, N. Demitri, R. Gambari, I. Lampronti, F. Rizzolio, C. Santo, F. Visentin, *Dalton Trans.* **2018**, *47*, 13616–13630; c) C. H. Wang, W.-C. Shih, H. C. Chang, Y.-Y. Kuo, W.-C. Hung, T.-G. Ong, W.-S. Li, *J. Med. Chem.* **2011**, *54*, 5245–5249; d) T. Scattolin, E. Bortolamiol, F. Rizzolio, N. Demitri, F. Visentin, *Appl. Organomet. Chem.* **2020**, *34*, e5876; e) T. Scattolin, E. Bortolamiol, I. Caligiuri, F. Rizzolio, N. Demitri, F. Visentin, *Polyhedron* **2020**, *186*, 114607.
[9] C. M. Zinser, F. Nahra, M. Brill, R. E. Meadows, D. B. Cordes, A. M. Z. Slawin, S. P. Nolan, C. S. J. Cazin, *Chem. Commun.* **2017**, *53*, 7990–7993.
[10] a) T. Scattolin, S. P. Nolan, *Trends Chem.* **2020**, *2*, 721–736; b) G. Pisanò, C. S. J. Cazin, *ACS Sustainable Chem. Eng.* **2021**, *9*, 9625–9631; c) T. Cauwenbergh, N. V. Tzouras, T. Scattolin, S. Bhandary, A. Simoens, C. V. Stevens, S. P. Nolan, *Chem. Eur. J.* **2021**, *27*, 13342–13345; d) N. V. Tzouras, F. Nahra, L. Falivene, L. Cavallo, M. Saab, K. Van Hecke, A. Collado, C. J. Collett, A. D. Smith, C. S. J. Cazin, S. P. Nolan, *Chem. Eur. J.* **2020**, *26*, 4515–1519; e) T. Scattolin, N. V. Tzouras, L. Falivene, L. Cavallo, S. P. Nolan, *Dalton Trans.* **2020**, *49*, 9694–9700; f) E. A. Martynova, N. V. Tzouras, G. Pisanò, C. S. J. Cazin, S. P. Nolan, *Chem. Commun.* **2021**, *57*, 3836–3856; g) N. V. Tzouras, E. A. Martynova, X. Ma, T. Scattolin, B. Hupp, H. Busen, M. Saab, Z. Zhang, L. Falivene, G. Pisanó, K. Van Hecke, L. Cavallo, A. Steffen, C. S. J. Cazin, S. P. Nolan, *Chem. Eur. J.* **2021**, *27*, 11904–11911.
[11] a) C. M. Zinser, K. G. Warren, R. E. Meadows, F. Nahra, A. M. Al-Majid, A. Barakat, M. S. Islam, S. P. Nolan, C. S. J. Cazin, *Green Chem.* **2018**, *20*, 3246–3252; b) C. M. Zinser, K. G. Warren, F. Nahra, A. Al-Majid, A. Barakat, M. S. Islam, S. P. Nolan, C. S. J. Cazin, *Organometallics* **2019**, *38*, 2812–2817; c) S. Ostrowska, T. Scattolin, S. P. Nolan, *Chem. Commun.* **2021**, *57*, 4354–4375.
[12] a) C. Sui-Seng, G. D. Enright, D. Zargarian, *Organometallics* **2004**, *23*, 1236–1246; b) D. Zargarian, *Coord. Chem. Rev.* **2002**, *233–234*, 157–176; c) P. R. Melvin, A. Nova, D. Balcells, W. Dai, N. Hazari, D. P. Hruszkewycz, H. P. Shah, M. T. Tudge, *ACS Catal.* **2015**, *5*, 3680–3688; d) Y. Liu, T. Scattolin, A. Gobbo, M. Beliš, K. Van Hecke, C. S. J. Cazin, S. P. Nolan, *Eur. J. Inorg. Chem.* **2022**, e202100840.
[13] a) D. Mavrynsky, J. Rahkila, D. Bandarra, S. Martins, M. Meireles, M. J. Calhorda, I. J. Kovács, I. Zupkó, M. M. Hänninen, R. Leino, *Organometallics* **2013**, *32*, 3012–3017; b) L. Dalla Via, S. Santi, V. Di Noto, A. Venzo, E. Agostinelli, A. Calcabrini, M. Condello, A. Toninello, *J. Biol. Inorg. Chem.* **2011**, *16*, 695–713; c) J. Honzíček, J. Vinklárek, Z. Padělková, L. Šebestová, K. Foltánová, M. Řezáčová, *J. Organomet. Chem.* **2012**, *716*, 258–268; d) O. Mrózek, L. Melounková, L. Dostál, I. Cisařová, A. Eisner, R. Havelek, E. Peterová, J. Honzíček, J. Vinklárek, *Dalton Trans.* **2019**, *48*, 11361–11373; e) O. Mrózek, L. Šebestová, J. Vinklárek, M. Řezáčová, A. Eisner, Z. Růžičková, J. Honzíček, *Eur. J. Inorg. Chem.* **2016**, 519–529.
[14] R. T. Baker, T. H. Tulip, *Organometallics* **1986**, *5*, 839–845.
[15] a) S. Grimme, C. Bannwarth, P. Shushkov, *J. Chem. Theory Comput.* **2017**, *13*, 1989; b) C. Bannwarth, S. Ehlert, S. Grimme, *J. Chem. Theory Comput.* **2019**, *15*, 1652.
[16] M. Adeel, S. Parisi, M. Mauceri, K. Asif, M. Bartoletti, F. Puglisi, I. Caligiuri, M. M. Rahman, V. Canzonieri, F. Rizzolio, *ACS Omega* **2021**, *6*, 28611–28619.
[17] E. Smolle, V. Taucher, J. Haybaeck, *Anticancer Res.* **2014**, *34*, 1553–1562.
[18] E. Kipps, D. S. P. Tan, S. B. Kaye, *Nat. Rev. Cancer* **2013**, *13*, 273–282.
[19] J. Kim, B.-K. Koo, J. A. Knoblich, *Nat. Rev. Mol. Cell Biol.* **2020**, *21*, 571–584.

[20] a) R. Perets, G. A. Wyant, K. W. Muto, J. G. Bijron, B. B. Poole, K. T. Chin, J. Y. Chen, A. W. Ohman, C. D. Stepule, S. Kwak, A. M. Karst, M. S. Hirsch, S. R. Setlur, C. P. Crum, D. M. Dinulescu, R. Drapkin, *Cancer Cell.* **2013**, *24*, 751–765; b) S. J. Hill, B. Decker, E. A. Roberts, N. S. Horowitz, M. G. Muto, M. J. Worley, C. M. Feltmate, M. R. Nucci, E. M. Swisher, H. Nguyen, C. Yang, R. Morizane, B. S. Kochupurakkal, K. T. Do, P. A. Konstantinopoulos, J. F. Liu, J. V. Bonventre, U. A. Matulonis, G. I. Shapiro, R. S. Berkowitz, C. P. Crum, A. D. D'Andrea, *Cancer Dis.* **2018**, *8*, 1404–1421; c) O. Kopper, C. J. de Witte, K. Lõhmussaar, J. E. Valle-Inclan, N. Hami, L. Kester, A. V. Balgobind, J. Korving, N. Proost, H. Begthel, L. M. van Wijk, S. A. Revilla, R. Theeuwsen, M. van de Ven, M. J. van Roosmalen, B. Ponsioen, V. W. H. Ho, B. G. Neel, T. Bosse, K. N. Gaarenstroom, H. Vrieling, M. P. G. Vreeswijk, P. J. van Diest, P. O. Witteveen, T. Jonges, J. L. Bos, A. van Oudenaarden, R. P. Zweemer, H. J. G. Snippert, W. P. Kloosterman, H. Clevers, *Nat. Med.* **2019**, *25*, 838–849.

[21] a) S. Palazzolo, M. Hadla, C. R. Spena, I. Caligiuri, R. Rotondo, M. Adeel, V. Kumar, G. Corona, V. Canzonieri, G. Toffoli, F. Rizzolio, *Cancers* **2019**, *11*, 1997; b) C. Granchi, G. Bononi, R. Ferrisi, E. Gori, G. Mantini, S. Glasmacher, G. Poli, S. Palazzolo, I. Caligiuri, F. Rizzolio, V. Canzonieri, T. Perin, J. Gertsch, A. Sodi, E. Giovannetti, M. Macchia, F. Minutolo, T. Tuccinardi, A. Chicca, *Eur. J. Med. Chem.* **2021**, *209*, 112857; c) T. Scattolin, E. Bortolamiol, F. Visentin, S. Palazzolo, I. Caligiuri, T. Perin, V. Canzonieri, N. Demitri, F. Rizzolio, A. Togni, *Chem. Eur. J.* **2020**, *26*, 11868–11876; d) F. Duzagac, G. Saorin, L. Memeo, V. Canzonieri, F. Rizzolio, *Cancers* **2021**, *13*, 1–35; e) T. Scattolin, E. Bortolamiol, S. Palazzolo, I. Caligiuri, T. Perin, V. Canzonieri, N. Demitri, F. Rizzolio, L. Cavallo, B. Dereli, M. V. Mane, S. P. Nolan, F. Visentin, *Chem. Commun.* **2020**, *56*, 12238–12241.

[22] D. Mustacich, G. Powis, *Biochem. J.* **2000**, *346*, 1–8.

[23] a) A. Bindoli, M. P. Rigobello, G. Scutari, C. Gabbiani, A. Casini, L. Messori, *Coord. Chem. Rev.* **2009**, *253*, 1692–1707; b) C. Gabbiani, G. Mastrobuoni, F. Sorrentino, B. Dani, M. P. Rigobello, A. Bindoli, M. A. Cinellu, G. Pieraccini, L. Messori, A. Casini, *MedChemComm* **2011**, *2*, 50–54; c) E. Schuh, C. Pflüger, A. Citta, A. Folda, M. P. Rigobello, A. Bindoli, A. Casini, F. Mohr, *J. Med. Chem.* **2012**, *55*, 5518–5528.

[24] a) C. Schmidt, B. Karge, R. Misgeld, A. Prokop, R. Franke, M. Brçnstrup, I. Ott, *Chem. Eur. J.* **2017**, *23*, 1869–1880; b) Y. Fuchita, H. Ieda, A. Kayama, J. Kinoshita-Nagaoka, H. Kawano, S. Kameda, M. Mikuriya, *Dalton Trans.* **1998**, 4095–4100; c) M. A. Cinellu, A. Zucca, S. Stoccoro, G. Minghetti, M. Manassero, M. Sansoni, *Dalton Trans.* **1995**, 2865–2872; d) P. Chakraborty, D. Oosterhuis, R. Bonsignore, A. Casini, P. Olinga, D.-J. Scheffers, *ChemMedChem* **2021**, *16*, 3060–3070.

[25] a) A. de Almeida, B. Oliveira, J. G. Correia, G. Soveral, A. Casini, *Coord. Chem. Rev.* **2013**, *257*, 2689–2704; b) B. Bertrand, A. de Almeida, E. P. M. van der Burgt, M. Picquet, A. Citta, A. Folda, M. P. Rigobello, P. Le Gendre, E. Bodio, A. Casini, *Eur. J. Inorg. Chem.* **2014**, 4532–4536; c) B. Bertrand, A. Citta, I. L. Franken, M. Picquet, A. Folda, V. Scalcon, M. P. Rigobello, P. Le Gendre, A. Casini, E. Bodio, *J. Biol. Inorg. Chem.* **2015**, *20*, 1005–1020; d) A. Casini, C. Hartinger, C. Gabbiani, E. Mini, P. J. Dyson, B. K. Keppler, L. Messori, *J. Inorg. Biochem.* **2008**, *102*, 564–75.

[26] a) Y. Tatsuno, T. Yoshida, S. Otsuka, *Inorg. Synth.* **1990**, *28*, 342–345; b) C. Sui-Seng, L. F. Groux, D. Zargarian, *Organometallics* **2006**, *25*, 571–579.

[27] A. Simoens, T. Scattolin, T. Cauwenbergh, G. Pisanó, C. S. J. Cazin, C. V. Stevens, S. P. Nolan, *Chem. Eur. J.* **2021**, *27*, 5653–5657.

[28] E. J. Baerends, D. E. Ellis, P. Ros, *Chem. Phys.* **1973**, *2*, 41–51.

[29] G. te Velde, F. M. Bickelhaupt, E. J. Baerends, C. F. Guerra, S. J. A. van Gisbergen, J. G. Snijders, T. Ziegler, *J. Comput. Chem.* **2001**, *22*, 931–967.

[30] E. J. Baerends, *Computer code ADF2019.305, SCM, Theoretical Chemistry*, Vrije Universiteit, Amsterdam, The Netherlands, **2019**.

[31] a) C. Lee, W. Yang, R. G. Parr, *Phys. Rev. B* **1988**, *37*, 785–789; b) A. D. Becke, *Phys. Rev. A* **1988**, *38*, 3098–3100.

[32] E. van Lenthe, E. J. Baerends, J. G. Snijders, *J. Chem. Phys.* **1994**, *101*, 9783–9792.

[33] a) M. Bortoli, S. M. Ahmad, T. A. Hamlin, F. M. Bickelhaupt, L. Orian, *Phys. Chem. Chem. Phys.* **2018**, *20*, 27592–27599; b) M. Dalla Tiezza, F. M. Bickelhaupt, L. Orian, *Chem. Open* **2019**, *8*, 143–154; c) M. Dalla Tiezza, F. M. Bickelhaupt, L. Orian, *ChemPhysChem* **2018**, *19*, 1766–1773; d) S. M. Ahmad, M. Dalla Tiezza, L. Orian, *Catalysts* **2019**, *9*, 679; e) L. Orian, F. M. Bickelhaupt, *Synlett* **2021**, *32*, 561–572; f) A. Madabeni, M. Bortoli, P. A. Nogara, J. B. T. Rocha, L. Orian, *Inorg. Chem.* **2021**, *60*, 4646–4656; g) L. Orian, W.-J. van Zeist, F. M. Bickelhaupt, *Organometallics* **2008**, *27*, 4028–4030.

[34] S. Grimme, S. Ehrlich, L. Goerigk, *J. Comput. Chem.* **2011**, *32*, 1456–1465.

[35] A. D. Becke, E. R. Johnson, *J. Chem. Phys.* **2005**, *123*, 154101.

[36] M. Franchini, P. H. T. Philipsen, L. Visscher, *J. Comput. Chem.* **2013**, *34*, 1819–1827.

[37] F. M. Bickelhaupt, E. J. Baerends, *Rev. Comput. Chem.* **2000**, *15*, 1–86.

[38] F. M. Bickelhaupt, K. N. Houk, *Angew. Chem. Int. Ed.* **2017**, *56*, 10070–10086; *Angew. Chem.* **2017**, *129*, 10204–10221.

[39] C. Fonseca Guerra, J.-W. Handgraaf, E. J. Baerends, F. M. Bickelhaupt, *J. Comb. Chem.* **2003**, *25*, 189–210.

[40] a) A. Klamt, G. Schüürmann, *J. Chem. Soc.-Perkin Trans.* **1993**, *2*, 799–805; b) A. Klamt, *J. Phys. Chem.* **1995**, *99*, 2224–2235.

[41] C. C. Pye, T. Ziegler, *Theor. Chem. Acc.* **1999**, *101*, 396–408.

[42] N. L. Allinger, X. Zhou, J. Bergsma, *J. Mol. Struct.* **1994**, *312*, 69–83.

[43] J. Lu, A. Vlamis-Gardikas, K. Kandasamy, R. Zhao, T. N. Gustafsson, L. Engstrand, S. Hoffner, L. Engman, A. Holmgren, *FASEB J.* **2013**, *27*, 1394–1403.

[44] A. Lausi, M. Polentarutti, S. Onesti, J. R. Plaisier, E. Busetto, G. Bais, L. Barba, A. Cassetta, G. Campi, D. Lamba, A. Pifferi, S. C. Mande, D. D. Sarma, S. M. Sharma, G. Paolucci, *Eur. Phys. J. Plus* **2015**, *130*, 1–8.

[45] W. Kabsch, XDS, *Acta Crystallogr. Sect. D* **2010**, *66*, 125–132.

[46] G. M. Sheldrick, *Acta Crystallogr. Sect. A* **2015**, *71*, 3–8.

[47] G. M. Sheldrick, *Acta Crystallogr. Sect. C* **2015**, *71*, 3–8.

[48] P. Emsley, B. Lohkamp, W. Scott, K. Cowtan, *Acta Crystallogr. Sect. D* **2010**, *66*, 486–501.

[49] L. Farrugia, *J. Appl. Crystallogr.* **2012**, *45*, 849–854.

[50] L. Schrodinger, *The PyMOL Molecular Graphics System* **2015**, http://www.pymol.org.

Manuscript received: February 15, 2022
Revised manuscript received: March 15, 2022
Accepted manuscript online: March 17, 2022